

Balanced optical-microwave phase detector for sub-femtosecond optical-RF synchronization

Michael Y. Peng,^{1,*} Aram Kalaydzhyan,² and Franz X. Kärtner^{1,2,3}

¹Department of Electrical Engineering and Computer Science and Research Laboratory for Electronics, Massachusetts Institute of Technology, 77 Massachusetts Avenue, Cambridge, MA 02139, USA

²Center for Free-Electron Laser Science, Deutsches Elektronen-Synchrotron, Germany

³Department of Physics, University of Hamburg and the Hamburg Center for Ultrafast Imaging, Luruper Chaussee 149, 22761 Hamburg, Germany

*mypeng@mit.edu

Abstract: We demonstrate that balanced optical-microwave phase detectors (BOMPD) are capable of optical-RF synchronization with sub-femtosecond residual timing jitter for large-scale timing distribution systems. RF-to-optical synchronization is achieved with a long-term stability of < 1 fs RMS and < 7 fs pk-pk drift for over 10 hours and short-term stability of < 2 fs RMS jitter integrated from 1 Hz to 200 kHz as well as optical-to-RF synchronization with 0.5 fs RMS jitter integrated from 1 Hz to 20 kHz. Moreover, we achieve a -161 dBc/Hz noise floor that integrates well into the sub-fs regime and measure a nominal 50-dB AM-PM suppression ratio with potential improvement via DC offset adjustment.

©2014 Optical Society of America

OCIS codes: (120.5050) Phase measurement; (120.3930) Metrological instrumentation; (320.7160) Ultrafast technology; (140.3425) Laser stabilization; (120.5790) Sagnac effect; (060.5625) Radio frequency photonics.

References and links

1. J. Kim, J. A. Cox, J. Chen, and F. X. Kärtner, "Drift-free femtosecond timing synchronization of remote optical and microwave sources," *Nat. Photonics* **2**(12), 733–736 (2008).
2. M. Y. Peng, P. T. Callahan, A. H. Nejadmalayeri, S. Valente, M. Xin, L. Grüner-Nielsen, E. M. Monberg, M. Yan, J. M. Fini, and F. X. Kärtner, "Long-term stable, sub-femtosecond timing distribution via a 1.2-km polarization-maintaining fiber link: approaching 10^{-21} link stability," *Opt. Express* **21**(17), 19982–19989 (2013).
3. M. Xin, K. Safak, M. Y. Peng, P. T. Callahan, and F. X. Kärtner, "One-femtosecond, long-term stable remote laser synchronization over a 3.5-km fiber link," *Opt. Express* **22**(12), 14904–14912 (2014).
4. J. Millo, M. Abgrall, M. Lours, E. M. L. English, H. Jiang, J. Guéna, A. Clairon, M. E. Tobar, S. Bize, Y. Le Coq, and G. Santarelli, "Ultralow noise microwave generation with fiber-based optical frequency comb and application to atomic fountain clock," *Appl. Phys. Lett.* **94**(14), 141105 (2009).
5. T. M. Fortier, M. S. Kirchner, F. Quinlan, J. Taylor, J. C. Bergquist, T. Rosenband, N. Lemke, A. Ludlow, Y. Jiang, C. W. Oates, and S. A. Diddams, "Generation of ultra-stable microwaves via optical frequency division," *Nat. Photonics* **5**(7), 425–429 (2011).
6. D. Li, M. Peng, H.-W. Chen, J. Lim, M. R. Watts, and F. Kärtner, "Fiber-Optic Demonstration of Optical Frequency Division for Erbium Silicon Photonics Integrated Oscillator," in *Conference on Lasers & Electro-Optics* (Optical Society of America, 2014), p. SF11.3.
7. K. Jung, J. Shin, and J. Kim, "Ultralow Phase Noise Microwave Generation From Mode-Locked Er-Fiber Lasers With Subfemtosecond Integrated Timing Jitter," *IEEE Photon. J.* **5**(3), 5500906 (2013).
8. V. Dolgovskiy, S. Schilt, N. Bucalovic, G. D. Domenico, S. Grop, B. Dubois, V. Giordano, and T. Südmeyer, "Ultra-stable microwave generation with a diode-pumped solid-state laser in the 1.5- μ m range," *Appl. Phys. B* **116**(3) 593–601 (2013).
9. A. Bartels, S. A. Diddams, C. W. Oates, G. Wilpers, J. C. Bergquist, W. H. Oskay, and L. Hollberg, "Femtosecond-laser-based synthesis of ultra-stable microwave signals from optical frequency references," *Opt. Lett.* **30**(6), 667–669 (2005).
10. K. J. Williams, R. D. Esman, and M. Dagenais, "Nonlinearities in p-i-n microwave photodetectors," *J. Lightwave Technol.* **14**(1), 84–96 (1996).
11. X. Xie, Q. Zhou, K. Li, A. Beling, and J. C. Campbell, "1.8 Watt RF Power and 60% Power Conversion Efficiency Based on Photodiode Flip-chip-bonded on Diamond," in *Conference on Lasers & Electro-Optics* (Optical Society of America, 2014), p. JTh5B.9.
12. T. M. Fortier, F. Quinlan, A. Hati, C. Nelson, J. A. Taylor, Y. Fu, J. Campbell, and S. A. Diddams, "Photonic microwave generation with high-power photodiodes," *Opt. Lett.* **38**(10), 1712–1714 (2013).

13. J. Taylor, S. Datta, A. Hati, C. Nelson, F. Quinlan, A. Joshi, and S. Diddams, "Characterization of Power-to-Phase Conversion in High-Speed P-I-N Photodiodes," *IEEE Photon. J.* **3**(1), 140–151 (2011).
 14. W. Zhang, T. Li, M. Lours, S. Seidelin, G. Santarelli, and Y. L. Coq, "Amplitude to phase conversion of InGaAs pin photo-diodes for femtosecond lasers microwave signal generation," *Appl. Phys. B* **106**(2), 301–308 (2012).
 15. W. Zhang, S. Seidelin, A. Joshi, S. Datta, G. Santarelli, and Y. Le Coq, "Dual photo-detector system for low phase noise microwave generation with femtosecond lasers," *Opt. Lett.* **39**(5), 1204–1207 (2014).
 16. F. Quinlan, F. N. Baynes, T. M. Fortier, Q. Zhou, A. Cross, J. C. Campbell, and S. A. Diddams, "Optical amplification and pulse interleaving for low-noise photonic microwave generation," *Opt. Lett.* **39**(6), 1581–1584 (2014).
 17. J. Kim, F. X. Kärtner, and F. Ludwig, "Balanced optical-microwave phase detectors for optoelectronic phase-locked loops," *Opt. Lett.* **31**(24), 3659–3661 (2006).
 18. J. Kim and F. X. Kärtner, "Attosecond-precision ultrafast photonics," *Laser Photon. Rev.* **4**(3), 432–456 (2010).
 19. K. Jung and J. Kim, "Subfemtosecond synchronization of microwave oscillators with mode-locked Er-fiber lasers," *Opt. Lett.* **37**(14), 2958–2960 (2012).
 20. M. Lessing, H. S. Margolis, C. T. A. Brown, P. Gill, and G. Marra, "Suppression of amplitude-to-phase noise conversion in balanced optical-microwave phase detectors," *Opt. Express* **21**(22), 27057–27062 (2013).
-

1. Introduction

Sub-femtosecond (sub-fs) synchronization between optical and radio-frequency (RF) sources is desirable for realizing a new regime of light and electron bunch control in next-generation light sources [1]. While recent developments in pulsed optical timing distribution systems are enabling sub-fs optical-to-optical synchronization across kilometer-scale distances for next-generation beamlines [2,3], it remains equally important to develop techniques to preserve these ultralow-noise optical signals into the RF domain for optical-to-RF synchronization.

Over the past few years, ultralow-noise microwave generation from optical frequency combs [4–8] have achieved such a high level of stability that it has become imperative to re-evaluate the methods for optical-RF conversion. Conventional methods using direct detection in standard photodiodes cannot achieve sub-fs performance due to nonlinearities at photodetection. Under high power illumination, the detector is subject to the space-charge effect, which limits the output RF power and increases the amplitude-to-phase (AM-PM) conversion noise [9,10]. Advanced detector designs can mitigate these effects to an extent. For example, untraveling-carrier diodes can achieve high linearity at output powers approaching the 1-W level [11] and low AM-PM conversion [12]. However, the conditions for the latter are highly sensitive to the average photocurrent and bias voltage [12–14], thus imposing difficulty for reliable operation in real systems. Various compensation techniques [15,16] can be implemented to improve aspects of direct detection, but the sensitivity of the AM-PM suppression remains at large for practical applications.

We adopt an alternative approach that is more robust to circumvent these issues. We developed a balanced optical-microwave phase detector (BOMPD) for an optoelectronic phase-locked loop (PLL) [17,18]. This PLL approach has two advantages. First, the BOMPD converts the phase error between an optical pulse train and RF signal into an amplitude-modulated signal directly in the optical domain. This signal can be detected via direct detection without concern for AM-PM conversion. Second, the phase error detection method by nature does not require as large of a dynamic range from the photodiode (hence, output power) as that of direct detection techniques to achieve the same level of synchronization.

Few groups have modified the basic BOMPD scheme with nonreciprocal biasing and balanced detection to improve the BOMPD noise floor down to -154 dBc/Hz and perform optical-RF extraction with sub-fs absolute timing jitter [19] as well as verify up to 60 dB of AM-PM suppression [20]. However, this modified scheme requires additional components that break the inherent symmetry of the Sagnac loop, thus degrading its long-term stability.

For this reason, we continued improving upon the basic BOMPD scheme [18]. Previously, our BOMPDs were limited to stability levels near the sub-10-fs regime. Here, we demonstrate that our improved BOMPDs can perform optical-to-RF (and RF-to-optical) synchronization with long-term-stable residual timing jitter in the sub-fs regime as well as achieve an AM-PM suppression ratio greater than 50 dB. This confirms the feasibility of BOMPDs for sub-fs synchronization in large-scale timing distribution systems in next-generation light sources.

2. Principle of operation

Optical-RF synchronization is performed using an optoelectronic PLL with a BOMPD as its phase detector – see Fig. 1. Its principle of operation is best understood first at the system-level as a PLL, then at the component-level for the BOMPD.

2.1 Optoelectronic phase-locked loop

The PLL begins with the two input signal sources: a mode-locked laser, which generates an optical pulse train with repetition rate f_r , and a VCO, which generates a single RF frequency near a multiple of the repetition rate $\sim Nf_r$. As a black box model, the BOMPD generates a voltage error signal ΔV that represents the phase error $\Delta\theta$ between the RF zero-crossings and pulse positions of the input signals. When $\Delta\theta$ is small, the output error signal is directly proportional to the input phase error according to $\Delta V = K_{PD} \cdot \Delta\theta$, where K_{PD} is the BOMPD phase sensitivity in units of Volts/rad. The error signal is sent to a proportional-integral loop filter and then fed back to the VCO frequency tuning port to complete the PLL. While this feedback configuration locks the VCO to the laser, the error signal can alternatively be fed back to the laser repetition rate to lock the laser to the VCO. In either situation, the PLL minimizes the error signal to zero. The loop filter is optimized to maximize the loop bandwidth and minimize the in-loop noise for tight synchronization.

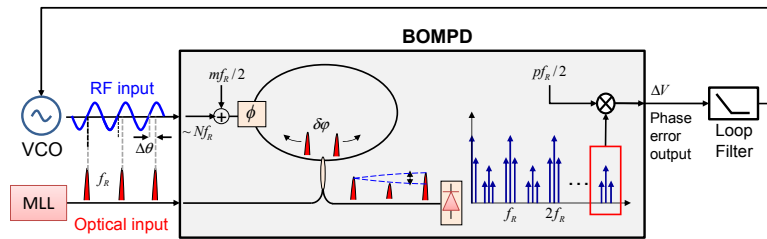


Fig. 1. Simplified schematic for an optoelectronic PLL to synchronize a VCO to a mode-locked laser (MLL). Gray inset shows a detailed schematic for the operation of the BOMPD as a phase detector. Assume $N = 1$ for simplicity.

2.2 Balanced optical microwave phase detector

Internal to the BOMPD is a fiber Sagnac interferometer (SGI), which is composed of a 50:50 coupler, fiber loop, and a unidirectional electro-optic phase modulator – see Fig. 1 [17]. Its operating principle is based on electro-optic sampling in the time domain – see Fig. 2:

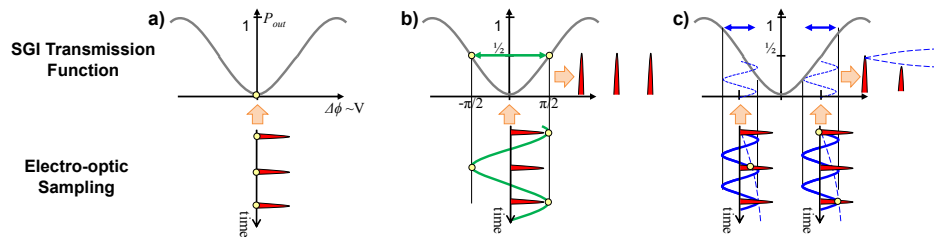


Fig. 2. Electro-optic sampling in the SGI for various modulator biasing conditions; (a) no RF signal applied, (b) reference bias signal applied for alternating quadrature bias, (c) VCO signal applied in addition to quadrature bias. Yellow dots indicate instances of electro-optic sampling.

Consider an input pulse, which is first split into two counter-propagating sub-pulses in the fiber loop. When no RF signal is applied to the modulator, the sub-pulses will accumulate a net zero differential phase $\delta\phi$ after one round-trip due to the loop symmetry. The sub-pulses will interfere upon exiting the loop and, according to the SGI transmission function $P_{OUT} = P_{IN} \sin^2(\delta\phi/2)$, result in zero transmission of the input pulse – see Fig. 2(a). This loop

symmetry is crucial because it passively biases the SGI at a fixed point in its transmission function, giving the BOMPD inherent robustness against long-term drifts.

A reference signal is then applied to prepare the SGI for phase detection. The SGI is biased at alternating quadrature points with opposite slope polarity – see Fig. 2(b). The quadrature bias maximizes the BOMPD phase sensitivity, while the alternating polarity generates a zero-crossing in the error signal necessary for phase-locking. The reference signal is derived from the input optical signal; the pulse train is detected, filtered at the m^{th} odd harmonic, and frequency-divided to a half-repetition-rate frequency $mf_r/2$. The signal is then time-delayed and amplified so that the clockwise sub-pulses, when passing through the modulator, will align with and “sample” the peak signal voltages to acquire alternating $\pm \pi/2$ phase shifts. The counterclockwise sub-pulses will acquire zero phase shifts in the modulator due to unidirectional modulation. The resulting net $\delta\phi = \pm \pi/2$ phase shifts will therefore achieve alternating quadrature bias. Note that the output pulse train with zero amplitude modulation serves as the reference level for the subsequent phase error detection.

The VCO signal is then applied in addition to detect its phase error relative to the pulse train. The pulses will sample the VCO signal at a slow difference frequency $\delta f = \text{mod}(\sim Nfr, fr)$, due to aliasing – see Fig. 2(c). Contrary to quadrature-biasing, the phase shifts acquired here typically have the same polarity for adjacent pulses; e.g. a positive (or negative) phase error drift will perturb the bias points to the right (or left), resulting in amplitude modulation of the output pulse train with the respective polarity. Upon detection, the modulated pulse train will contain error sidebands centered at the half-repetition rate frequencies. One set of sidebands is filtered and down-mixed in-phase with another reference signal to generate the baseband voltage error signal. Further detailed description of the SGI can be found in [17].

2.3 Design considerations

A few important design considerations are emphasized here. First, contrary to our previous work, the reference signal is increased into the multi-GHz regime to achieve unidirectional modulation in the phase modulator. Since the arrival time of counterclockwise sub-pulses in the modulator is no longer important, the SGI becomes repetition-rate independent and is more robust against imperfect loop lengths and environmental noise.

Second, as intentionally designed, the only PM-sensitive path in the BOMPD to first-order approximation is the VCO signal path. All other signal paths, i.e. reference signal generation, quadrature biasing, and error signal detection, are AM-sensitive. The electronics for these signal paths are optimized accordingly.

Third, the VCO signal is amplified beyond V_π of the phase modulator to increase its zero-crossing slope to maximize K_{PD} . Although this generates higher-order nonlinearities in the error signal, they can be ignored because the PLL locks only to the zero-crossing where linearity is preserved. Moreover, the resultant null error signal poses no risk for saturation or nonlinearities in the detection electronics. This fundamentally differs from conventional phase detection methods where the signal power at the RF port of a RF mixer is always present and contends with the LO power to maximize phase sensitivity while avoiding mixer nonlinearity.

3. Optical-RF synchronization demonstrations

BOMPDs are used within a timing distribution system for two purposes: 1) central-station locking, where the optical signal source for timing distribution is first synchronized to a local ultra-stable RF reference, and 2) remote-station locking, where remote RF oscillators are synchronized to the optical timing signal delivered from the central station. We experimentally demonstrate both scenarios and verify the capability of BOMPDs for sub-fs synchronization. For the scope of this paper, we omit the timing-stabilized polarization-maintaining fiber links [2,3] used to distribute the timing signal for remote-station locking.

3.1 Experimental set-up

A typical experimental set-up is shown in Fig. 3. We provide a detailed description of the remote-station locking set-up and note key system changes as necessary for the remaining system demonstrations in this paper.

The input pulse train is generated from a free-running Er-doped mode-locked laser (Menlo Systems; M-comb) that outputs 170-fs pulses centered at 1558 nm with a 200.4-MHz fundamental repetition rate. The pulses are split into the reference path and main SGI path. The reference path contains a high-speed 14-GHz photodiode (Discovery Semi; DSC40S), narrow bandpass filter (TTE) for the 63rd harmonic of the pulse train, and divide-by-2 digital frequency divider (Hittite; HMC492LP3) to generate a reference signal at 6.3 GHz. The optical power to the reference path is limited to 0 dBm to avoid detector saturation. Low noise amplifiers, variable RF attenuators, and phase shifters are employed as necessary to achieve quadrature bias. The main SGI path is constructed using polarization-maintaining fiber components, namely a 50:50 coupler (AFW) and 10-GHz phase modulator (EOSpace). Dispersion-compensating fiber is essential for minimizing the pulse width at the modulator input for high-accuracy electro-optic sampling.

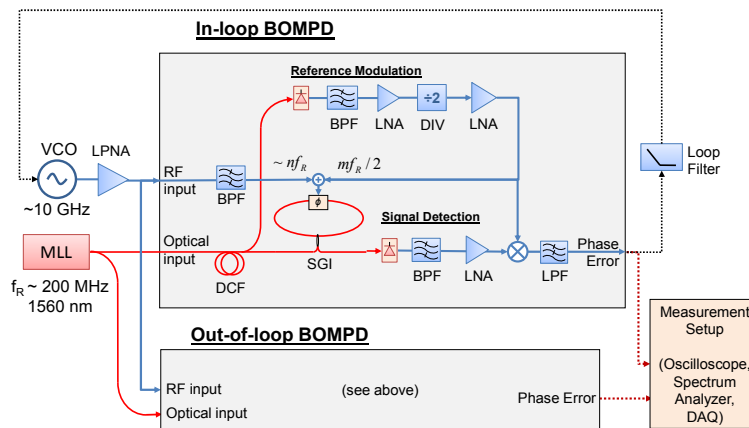


Fig. 3. Detailed experimental set-up for RF-to-optical synchronization. Second BOMPD is for an out-of-loop residual phase error measurement; MLL, mode-locked laser; BPF, bandpass filter; LNA, low noise amplifier; DIV, frequency divider; LPF, lowpass filter, LPNA, low phase noise amplifier; DCF, dispersion-compensation fiber; DAQ, analog-to-digital converter

With the BOMPD biased at quadrature, the VCO (PSI; DRO-10.225-FR), which is to be phase-locked to the 51st harmonic (10.220 GHz) of the pulse train, is then added to the phase modulator using a RF diplexer. To maximize the BOMPD phase sensitivity, the VCO signal is amplified with a low phase noise amplifier (Microsemi; AML1011PNB3001) to just below the damage threshold of the modulator at +24 dBm. An additional noise filter may be necessary post-amplification to suppress the amplified broadband noise; this noise will be aliased down to baseband during electro-optic sampling and may degrade the BOMPD noise floor. At the SGI output, the modulated pulse train is then detected with -3 dBm of power on another high-speed photodiode (Discovery Semi; DSC50S), filtered at 6.3 GHz (K&L; 6C60-6360/T100-O/O), amplified and down-converted in-phase with the reference signal in an RF mixer to generate the baseband error signal. The incident optical power and RF gain in the signal detection path is set to maximize the signal-to-noise ratio (SNR) and linearity. A proportional-integral controller (Vescent; D2-125) feeds the error signal back to the VCO tuning port to close the PLL with a 100-kHz locking bandwidth.

To characterize the PLL performance, a second nearly identical BOMPD is implemented for an out-of-loop measurement. The out-of-loop BOMPD is configured with a lower noise floor than the in-loop BOMPD to allow for direct observation of the in-loop performance. Low-noise DC preamps with 36-dB gain are used to amplify the error signals above the

measurement noise floor. The in-loop and out-of-loop BOMPD sensitivities measured at the input to the measurement set-up are 4.4 mV/fs and 4.8 mV/fs, respectively, referred to 10.220 GHz. For long-term drift measurements, the out-of-loop error signal is low-pass filtered at 1 Hz and sampled at 1 Hz with an analog-to-digital converter. Temperatures at various locations in the set-up are also recorded. For short-term jitter measurements, both error signals are measured with a spectrum analyzer from 1 Hz to 1 MHz. The voltage measurements are converted to phase using the BOMPD phase sensitivity K_{PD} , which is directly measured from the zero-crossing slope of the error signal when the PLL is unlocked. Short-term measurements are confirmed with a phase noise model of the optoelectronic PLL.

3.2 Remote station locking: VCO to MLL

For remote-station locking, the VCO is locked to a mode-locked laser with lower noise performance. Short-term stability measurements are shown in Fig. 4. The free-running phase noise spectra of the signal sources are shown in black for reference. The VCO phase noise is obtained via a loose phase-lock with a second identical VCO in a conventional dual-oscillator phase noise measurement set-up. The laser phase noise is obtained via direct detection and measurement of the 10.220 GHz harmonic with a signal source analyzer. The residual phase error as measured by the in-loop and out-of-loop BOMPDs while the PLL is locked are shown in blue and red, respectively. Noise contributions to the BOMPD noise floor are carefully characterized. This is essential because it enables independent assessment of the BOMPD's limitations for phase detection and that of the PLL's limitations for the overall optical-RF synchronization. The latter is highly dependent on the choice of signal sources and locking parameters, which are external to the BOMPD.

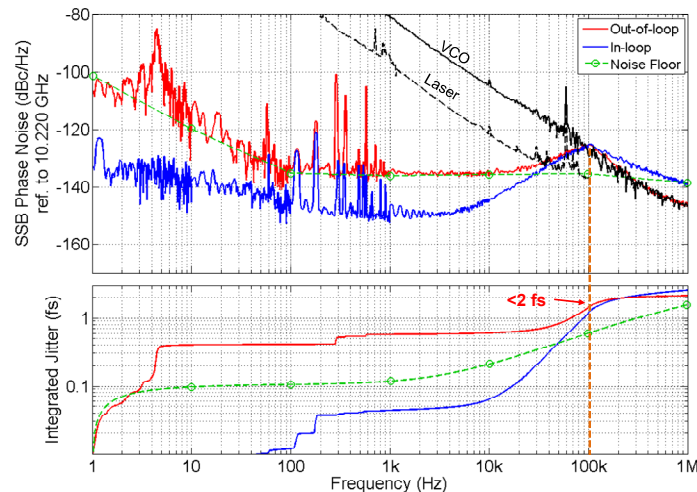


Fig. 4. Short-term residual phase error measurements for remote-station locking referred to 10.220 GHz (top) and its corresponding integrated RMS timing jitter starting from 1 Hz (bottom); Free-running phase noise of the VCO and laser are shown in black. Out-of-loop integrated jitter is <2 fs for a 100-kHz locking bandwidth.

With our improved BOMPDs, RF-to-optical synchronization is for the first time limited by the photodetection noise floor in the in-loop BOMPD (see green curve). The detection noise floor contains two dominant power-law noise processes. The white noise floor above 100 Hz represents thermal noise at detection, while the f^{-2} behavior below 100 Hz represents colored noise from the electronics. Exceptions to these trends are noise spurs from ground loops (multiples of 60 Hz), particular RF components (200-600 Hz) and vibrations (near 6 Hz). The corresponding integrated timing jitter for the residual phase error spectra are shown at the bottom of Fig. 4. The integrated BOMPD noise floor shows potential for sub-fs synchronization up to a 300-kHz locking bandwidth. Even if noise spurs from the red curve

are included, which total 0.6 fs RMS between 1 Hz and 1 kHz, the sub-fs range is degraded to only 200 kHz. This locking bandwidth is still sufficient for synchronizing most high-end commercial oscillators. For this locking demonstration, the out-of-loop timing jitter integrated from 1 Hz to the 100-kHz locking bandwidth is just below 2 fs RMS. This can easily be improved into the sub-fs regime by using a lower-noise VCO. Another option would be to optimize the PLL phase margin to extend the locking bandwidth; however, this is challenging due to un-modelled higher-order zeroes and poles in the detection electronics that generate an unstable resonance near 1 MHz.

It is necessary to understand that the observed thermal noise floor is not yet a fundamental limit for the BOMPD. A figure of merit for the BOMPD is the SNR at detection. The noise floor can be effectively suppressed by increasing the signal power, or equivalently K_{PD} . This is demonstrated in sections 3.3 and 3.4 by increasing the power incident on the detector and decreasing the down-conversion frequency for higher detector responsivity.

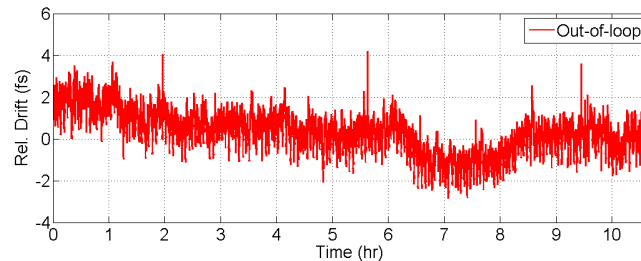


Fig. 5. Long-term drift measurement for remote-station locking referred to 10.220 GHz. Out-of-loop curve shows 1 fs RMS drift and < 7 fs pk-pk over 10 hours of uninterrupted operation, and 0.8 fs RMS drift over the first 6 hours.

We also demonstrate long-term stability with 1.0 fs RMS and < 7 fs pk-pk drift for over 10 hours of continuous operation and 0.8 fs RMS over the first 6 hours – see Fig. 5. This is over a factor of 5 improvement from our previous work at 5.18 fs RMS [18]. Although this is comparable to that recently reported in [19], the long-term drift of the modified SGI is caused in the optical domain by coupling ratio drifts, beam drifts, and imbalanced attenuation. Our simplified SGI is insensitive to such drifts. Instead, drift is caused by environmental perturbations to the mechanical stability of the electronics; vibrations from heat sink fans, mechanical stress, and thermal expansion induce length changes in the RF signal paths, which translate into non-negligible phase drifts, especially for high-frequency signals. The high correlation between timing drift and ambient temperature is measured at 0.7. Localized heating of specific signal paths was performed to verify this. Preventative measures against temperature- and vibration-induced drifts are taken, such as replacing RF cables with rigid connectors, securing components to the breadboard, and placing lead foam beneath the set-up. However, due to the large set-up and overheating of the RF power amplifiers, no isolated temperature enclosure is used. Higher-frequency noise from ground loops and electro-static discharge spikes are still observed despite using a 1-Hz lowpass filter; e.g. a strong noise source is recorded near 4.5 mHz with an RMS value of 0.5 fs. The analog-to-digital converter is suspected of aliasing ground-loop noise down to baseband. With proper optimization of the electronics, this noise should be eliminated.

3.3 Central station locking: MLL to SLCO

For central-station locking, the signal sources are exchanged for a Sapphire-loaded cavity oscillator, SLCO (Raytheon; SLCO-10.833-NCS) and another mode-locked laser (OneFive; Origami) whose 216.667-MHz repetition rate is compatible with the 10.833 GHz SLCO frequency. The error signal feedback is reconfigured to lock the laser to the SLCO. Moreover, the RF power amplifier in the reference path is upgraded to one with superior AM noise performance (CiaoWireless; CA67-345-LP-HB). The remaining set-up is left unmodified. The in-loop and out-of-loop BOMPD sensitivities are 6.0 mV/fs and 5.2 mV/fs, respectively,

referred to 10.833 GHz. For tight synchronization, the residual phase error spectra in Fig. 6 shows a loop bandwidth limited to 20 kHz as well as a moderate servo resonance. These arise from the laser PZT resonance close in at 30 kHz, which degrades the PLL locking bandwidth and phase margin. Despite this, the out-of-loop integrated jitter is only 0.5 fs from 1 Hz to 20 kHz, which is in the sub-fs regime. Due to higher signal power available from the laser, the effective noise floor is improved, thus extending the potential for sub-fs synchronization beyond 1 MHz. PLL performance is again limited by the in-loop detection noise floor. The new low-frequency behavior obeys the f^{-1} flicker noise of the replacement amplifier.

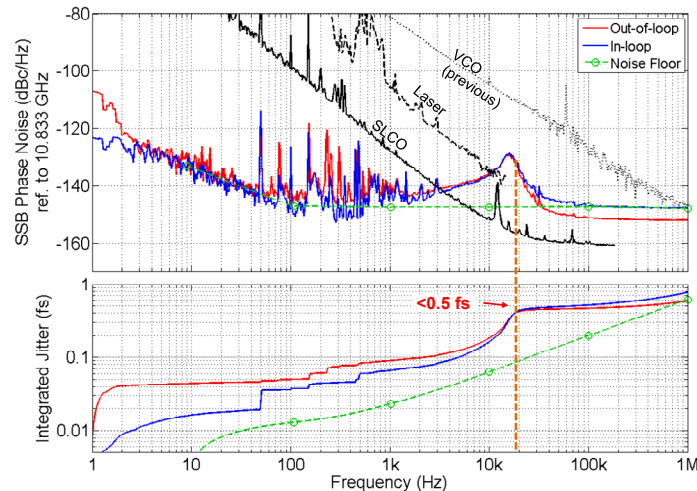


Fig. 6. Short-term residual phase error measurements for central-station locking referred to 10.833 GHz (top) and its corresponding integrated RMS timing jitter starting from 1 Hz (bottom); Free-running phase noise of the SLCO and laser are shown in black. Out-of-loop integrated jitter is < 0.5 fs for a 20-kHz locking bandwidth. Noise floor data below 10 Hz is discarded due to data acquisition error.

3.4. BOMPD noise floor suppression

The BOMPD noise floor can be suppressed further by increasing the SNR at photodetection. Although a high-frequency reference signal is advantageous for repetition-rate independence in the SGI, it is disadvantageous for error signal detection since the detector responsivity and saturation are lower at high frequencies. To maximize detector responsivity, the 6.3-GHz electronics in section 3.3 are replaced to perform down-conversion at 108.333 MHz, the lowest half-repetition-rate possible. To maximize RF signal power, the power incident on the detector is increased to +5 dBm, which is near saturation for 108.333 MHz.

The experimental set-up is optimized to achieve the minimum noise floor possible for a single BOMPD with the PLL unlocked and VCO signal removed. The expected improvement in SNR is verified in Fig. 7, which shows the direct measurement of a -161 dBc/Hz detection noise floor referred to 10.833 GHz. The integrated jitter up to 1 MHz is just below 0.2 fs, which shows great potential for sub-fs synchronization over large locking bandwidths. Few noise spurs still exist, such as 60 Hz power line noise, a 500 Hz spur due to particular electronics and a drifting tone near 700-800 Hz due to parasitic pick-up of the SLCO signal through air. Their contribution to the overall jitter is, however, negligible. The white noise floor represents shot noise from the higher photocurrent, and the f^{-3} low-frequency noise represents noise from the low-frequency detection electronics. The white noise floor can be improved by using a high-power linear diode [11] to increase the RF signal power at photodetection by +20 dB, which would yield a noise floor below -180 dBc/Hz. Long-term stability is expected to improve since the lower detection frequency decreases the BOMPD's sensitivity to temperature-induced phase shifts; i.e., by switching from 6.3 GHz to 108 MHz,

the effective phase change for a given temperature-induced length fluctuation would decrease by a factor of nearly 60.

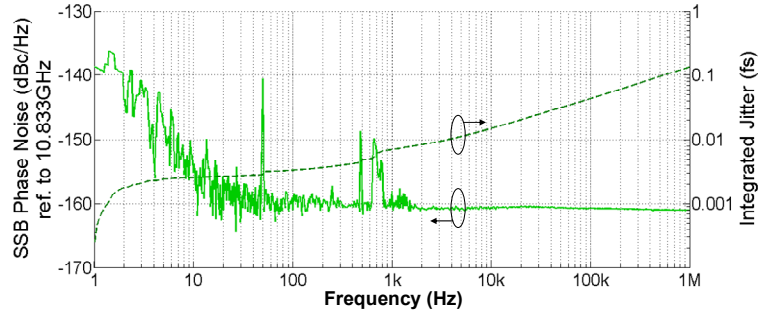


Fig. 7. Improved BOMPD noise floor using low-frequency detection electronics for increased signal power. The -161 dBc/Hz noise floor corresponds to an integrated sub-fs noise floor well beyond 1 MHz.

4. AM-PM suppression measurement

Another figure of merit for the BOMPD is the AM-PM suppression ratio. To measure this, the optical input to the BOMPD is amplitude-modulated with an electro-optic modulator while the resultant phase-modulation at the BOMPD output is monitored. The RF synthesizer driving the modulator is swept from 100 Hz to 1 MHz. The input relative intensity noise spectrum in dBc/Hz is subtracted from the output phase noise spectrum in dBrad²/Hz to calculate the AM-PM suppression ratio. This ratio can also be reported as α in linear units of rad/($\Delta I/I$). Contrary to traditional AM-PM conversion processes, we measure here the leakage of input AM noise to the output AM noise and use K_{PD} to convert this AM-AM leakage into an AM-PM conversion coefficient.

Measurements are performed with the PLL in both the on and off states. In the “PLL off” state, the VCO signal is not applied during measurement, but is applied afterwards to obtain K_{PD} . As shown in Fig. 8, the BOMPD exhibits a wideband flat -50 dB of AM-PM suppression (see red curve), or equivalently $\alpha = 0.003$ rad. In the “PLL on” state, the measurement is performed while the VCO is phase-locked to the laser with a 10-kHz locking bandwidth (see blue curves). This technique is similar to that conventionally used for characterizing the closed-loop response of a PLL. For frequencies well beyond the locking bandwidth, i.e. above 20 kHz, the PLL response behaves as a unity-gain high-pass function. However, we observe that fine adjustment of the DC offset on the order of a few mV in the loop filter can improve the AM-PM suppression ratio beyond 50 dB. This is possible because the DC offset compensates for imperfections in the SGI, which may result from AM noise in the quadrature-biasing and finite polarization extinction ratio. Future work will be to verify this DC offset dependency with an independent out-of-loop measurement.

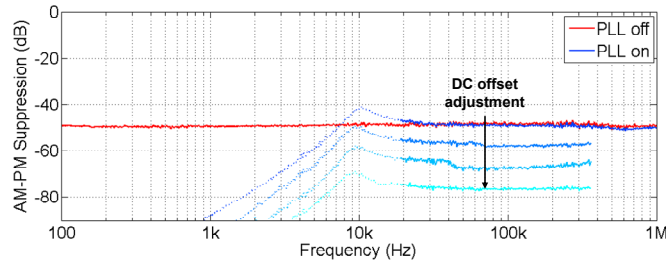


Fig. 8. AM-PM suppression measurement with the PLL unlocked (red) and locked (blue). BOMPD exhibits a nominal wideband -50 dB (or $\alpha = 0.003$ rad) AM-PM suppression with improvement via DC offset adjustment.

To investigate the source of AM-PM conversion, the reference and main SGI paths are modulated independently. Modulation of the reference path yields an AM-PM suppression that is limited by the measurement noise floor, which is greater than 90 dB. This is expected because the digital frequency divider used for reference signal generation is insensitive to AM noise at its input and able to generate an isolated waveform with low AM noise at its output. These effects compound favorably to decouple the input AM noise from the output PM noise. Modulation of the SGI path, however, reproduced the 50-dB suppression. This confirms that the AM-PM conversion is limited by optical AM-AM leakage in the SGI. Future work will be to investigate the fundamental limit for this leakage and improve the suppression ratio. Although our nominal 50-dB suppression ratio is currently 10 dB lower than that in [20], the immediate benefit of our simplified BOMPD is the improvement in long-term stability due to the increased robustness of the SGI from imperfect balancing. Moreover, both BOMPDs still offer a suppression ratio that is significantly higher and more robust than that of direct detection, as discussed below.

We further show that the AM-PM suppression ratio is reliable with respect to large changes in optical power. Although K_{PD} varies directly with power changes, the AM-AM leakage remains constant because it is due to fixed optical power attenuation from the imperfect biasing of the SGI. The effective AM-PM suppression ratio therefore changes as a linear function of optical power. This was experimentally verified by varying the optical power over several dBs and observing commensurate changes in the AM-PM suppression ratio from its nominal 50-dB value. This is in contrast to direct detection techniques, such as [12], where the minimum AM-PM suppression exists only at localized points for select bias voltages and average photocurrents; local minima values for α , which may vary from 0.04 to 2 rad (or -30 to $+6$ dB), can only be maintained if power fluctuations remain within a small percentage. The BOMPD is a more robust method for low AM-PM conversion in optical-RF synchronization systems where the optical power may differ greatly throughout a facility.

5. Conclusion

By characterizing noise sources within the BOMPD and systematically optimizing the optics and electronics, we were able to improve the BOMPD noise floor into the sub-fs regime. In the series of experiments presented, we first achieved RF-to-optical synchronization with a long-term stability of < 1 fs RMS drift and < 7 fs pk-pk for over 10 hours and short-term stability of < 2 fs RMS jitter integrated from 1 Hz to 200 kHz, followed by optical-to-RF synchronization with 0.5 fs RMS jitter integrated from 1 Hz to 20 kHz. We then optimized a single BOMPD to achieve a noise floor of -161 dBc/Hz, which integrates well into the sub-fs regime for large locking bandwidths beyond 1 MHz. Future work is planned to improve the noise floor by increasing the SNR at detection. Lastly, we measured a nominal, wideband AM-PM suppression ratio of 50 dB with potential improvement via DC offset adjustment. These results confirm the feasibility of BOMPDs for sub-fs optical-RF synchronization in large-scale timing distribution systems for next-generation light sources.

Acknowledgments

The authors acknowledge financial support by the United States Department of Energy through contract DE-SC0005262, and the Center for Free-Electron Laser Science at Deutsches Elektronen-Synchrotron, Hamburg, a research center of the Helmholtz Association, Germany and by the excellence cluster “The Hamburg Centre for Ultrafast Imaging-Structure, Dynamics and Control of Matter at the Atomic Scale” of the Deutsche Forschungsgemeinschaft.